Elemental Photocatalysts

DOI: 10.1002/ange.201302238

Visible-Light-Responsive β-Rhombohedral Boron Photocatalysts**

*Gang Liu, Li-Chang Yin, Ping Niu, Wei Jiao, and Hui-Ming Cheng**

Photocatalytic solar-energy conversion has been attracting worldwide attention owing to its great significance in the provision of renewable energy and protection of the environment.[1–3] As important as the tailoring of well-known photocatalysts, such as TiO_2, for high photocatalytic efficiency[4–7] is the investigation of unknown semiconductor photocatalysts.[8–16] So far, hundreds of photocatalysts have been examined, most of which have been compounds.[3,17,18] Recently, elemental semiconductors (Si, Se, P, S) have emerged as an attractive class of photocatalysts owing to their visible-light response and suitable band edges for targeted photocatalysis reactions.[19–24] It is logical to also anticipate the use of elemental boron in photocatalysis because of its semiconducting properties. When we investigated β-rhombohedral boron crystals with and without an amorphous oxide layer on their surface, we discovered that the crystals were indeed photocatalytically active under visible light, and that the existence of a surface amorphous oxide layer substantially impaired their photocatalytic activity. The findings in this study may open a door to the development boron-based photocatalysts.

Boron has aroused wide interest owing to its fascinating properties (light weight, high strength, high hardness, high melting point, high chemical resistance, typical semiconductivity, and superconductivity at high pressure), although a pure phase was not obtained until 1909.[25–27] It has at least 17 polymorphs (or more precisely, boron-rich compounds) as a result of electron-deficient bonding.[28] All polymorphs contain B_{12} icosahedral clusters as a basic building block (see the inset in Figure 1a). Among these polymorphs, α-tetragonal, α-rhombohedral, β-tetragonal, and β-rhombohedral boron are the four main forms under ambient conditions. Experimentally, β-rhombohedral boron is the most thermodynamically stable form, although its superior stability was not supported by theoretical investigations until 2007.[29–31] This long-term discrepancy stems from the difference between the idealized structural model of 105 boron atoms (B_{105}) that is used to describe the β-rhombohedral form and the real structure, which contains partially occupied sites. As a consequence, the theoretically predicted metallic property does not agree with the experimentally derived p-type semiconducting behavior of β-rhombohedral boron with a proposed bandgap of 1.5–1.6 eV.[32] Improved crystallographic studies and optimized theoretical structure models have reduced the gap between experiment and theory to some extent and provided a strong background for the further investigation of structure–property relationships and the exploration of new uses for β-rhombohedral boron.

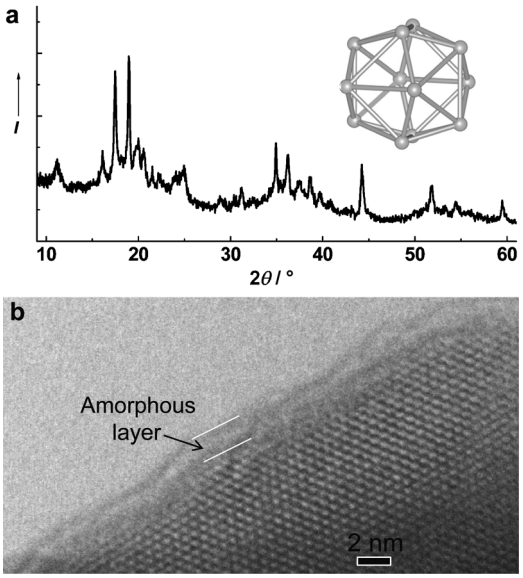

Figure 1. Structure characterization: a) XRD pattern of sub-micrometer-sized β-rhombohedral boron. b) High-resolution TEM image recorded at the edge of a sub-micrometer-sized β-rhombohedral boron particle. The inset in (a) shows the structure of an icosahedral B_{12} cluster.

The bandgap of 1.5–1.6 eV indicates that β-rhombohedral boron should respond to visible light over a wide range of wavelengths. It was also found in quasi-four-electrode measurements that β-rhombohedral boron exhibited strong photoconductivity under illumination by a halogen lamp or argon-ion laser (at 488 nm).[26] Encouraged by these favorable properties, we investigated the photocatalytic activity of two kinds of commercially available β-rhombohedral boron crystals (sub-micrometer-sized and micrometer-sized) by structural characterization, measurement of their optical properties, and theoretical calculation of their electronic structures.

Figure 1a shows the X-ray diffraction (XRD) pattern of sub-micrometer-sized boron powder. All diffraction peaks can be assigned to β-rhombohedral boron (JCPDS: 11-0618; space group: $R\bar{3}m$ (166); $a = 10.952$ Å, $c = 23.824$ Å). Besides the sharp peaks, there are several diffuse peaks in the background, which indicate the existence of amorphous

[*] Dr. G. Liu, Dr. L.-C. Yin, P. Niu, W. Jiao, Prof. H.-M. Cheng
Shenyang National Laboratory for Materials Science
Institute of Metal Research, Chinese Academy of Sciences
72 Wenhua Road, Shenyang 110016 (China)
E-mail: cheng@imr.ac.cn

[**] We thank the Major Basic Research Program, Ministry of Science and Technology of China (No. 2009CB220001), the NSFC (No. 50921004, 51002160, 21090343, 51172243, 51202255), and the Chinese Academy of Sciences (KJCX2-YW-H21-01) for financial support. L.-C.Y. acknowledges support from Shenyang Supercomputing Center, CAS.

Supporting information for this article is available on the WWW under http://dx.doi.org/10.1002/anie.201302238.

structures. The microstructure shown in Figure 1b of a sub-micrometer-sized boron particle indicates that the particle consists of a highly crystalline inner region and an amorphous surface layer with a thickness of around 2 nm; these observations are consistent with the XRD results.

The composition and chemical state of the surface layer of the sub-micrometer-sized and micrometer-sized boron crystals were determined by X-ray photoelectron spectroscopy (XPS). Boron and oxygen exist in both crystals, as shown in Figure 2. For the sub-micrometer-sized crystal, the peak with

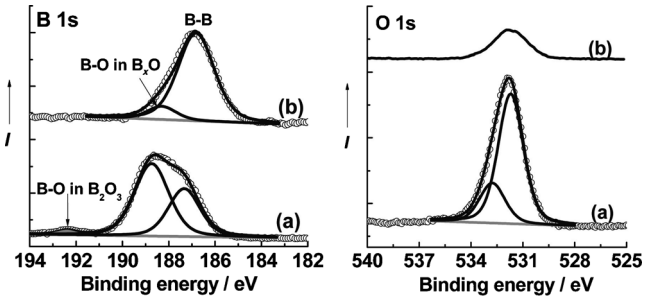

Figure 2. Chemical states: High-resolution B 1s and O 1s XPS spectra recorded from the pristine surface of a) sub-micrometer-sized β-rhombohedral boron and b) micrometer-sized β-rhombohedral boron.

its center at 187.3 eV in the B 1s XPS spectrum is typically attributed to the B–B bonds of elemental boron.[33] The strongest peak centered at 188.8 eV is assigned to the B–O bonds in boron-rich oxides, in which an oxygen atom is coordinated by several boron atoms (B_x–O).[33] This boron species gives a corresponding strong O 1s XPS signal with its center at 531.7 eV. The minor B 1s XPS peak at a higher binding energy of 192.4 eV is related to the B–O bonds in B_2O_3[33] and corresponds to the O 1s feature at 532.8 eV. The atomic ratio of oxygen to boron in the sub-micrometer-sized particles is as high as 1:1.5. All these results confirm that the surface amorphous layer revealed by XRD and the high-resolution TEM image in Figure 1 is composed of boron-rich oxides.

In contrast to the sub-micrometer-sized boron species, the micrometer-sized boron is highly crystalline, as indicated by the sharp diffraction peaks in the XRD pattern (see Figure S1 in the Supporting Information). The substantially weakened B 1s XPS B_x–O peak suggests the absence of a boron-rich-oxide-based surface amorphous layer. The B–B bond B 1s feature with its binding energy of 186.8 eV becomes dominant, and the ratio of oxygen to boron decreases to 1:6.3. The binding energy of the B_x–O B 1s feature in the micrometer-sized boron is apparently shifted towards a lower energy relative to that observed for the sub-micrometer-sized boron (188.3 versus 188.8 eV), probably as a result of the low extent of boron oxidation when the oxygen content is lower.

The optical properties of the boron sample were studied by UV/Vis absorption spectroscopy. The sub-micrometer-sized boron has an absorption edge up to 800 nm (Figure 3a). The absorption onset determined from the plot of the transformed Kubelka–Munk function versus the energy of light (Figure 3b) is 1.66 eV. This value seems to be in

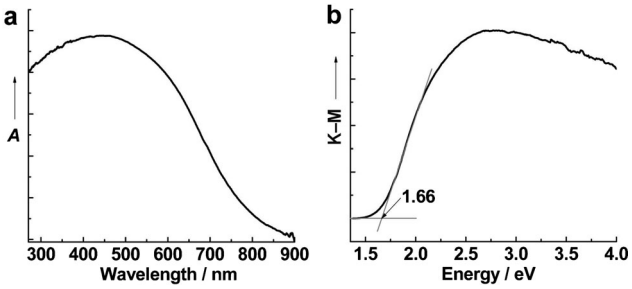

Figure 3. Optical properties: a) UV/Vis absorption spectrum of the sub-micrometer-sized boron. b) Plot of the transformed Kubelka–Munk function, $(F(R)h\nu)^2$, against the energy of light.

agreement with the reported bandgap of β-rhombohedral boron.[32] To gain an understanding of the above optical properties, we conducted first-principles calculations of the electronic structures of β-rhombohedral boron. The crystal structure of β-rhombohedral boron is quite complex, and various models have been proposed to address the relative stability of the α and β forms. It is generally accepted that the structure of B_{105} (namely, Pearson-type hR105),[34] in which 105 boron atoms fully occupy the 105 lattice sites of the unit cell, does not reflect the real structure of β-rhombohedral boron. Further investigations led to the agreement that the real structure is partially occupied.[29–31,35] Pearson-type hR141 consisting of 20 Wyckoff positions labeled B1–B20 is one such model, in which approximately 107 atoms are distributed among 141 sites (Figure 4a).[36] Theoretical studies

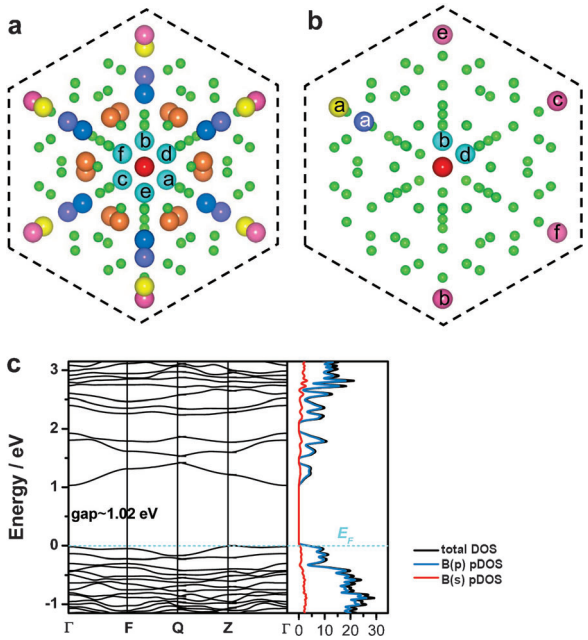

Figure 4. Atomic and electronic structure: a) Structure of β-rhombohedral boron (Pearson-type hR141) in the vicinity of a cell body center (B15, shown in red) as viewed along the rhombohedral (111) axis. Partially occupied sites are shown in color: B13 pink, B16 cyan, B17 yellow, B18 indigo, B19 blue, B20 orange.[36] b) Structure of β′-hR141 boron with partial occupancy as $B13_{bcef}B16_{ba}B17_aB18_a$. c) Calculated electronic band structure (left) and density of states (DOS; right) for β′-hR141 boron. E_F = Fermi energy; pDOS = partial density of states.

on the stability of boron structures revealed that a superstructure of boron, namely, β′-hR141 boron with a partial occupancy $B13_{bcef}B16_{bd}B17_{a}B18_{a}$ (see Figure 4b), can be obtained by optimizing the site occupation.[36] The energy of this superstructure is lower than that of the α form, but its symmetry is lower than that of the β form. Therefore, we chose β′-hR141 boron as a model structure to calculate the electronic properties of boron.

Figure 4c shows the calculated band structure of β′-hR141 boron. Both conduction and valence bands with wide dispersions are mainly contributed by boron p orbitals. A direct bandgap of 1.02 eV at the Γ point, which is smaller than the experimentally determined value (1.66 eV) due to the well-known bandgap underestimation within the framework of standard density functional theory, could be responsible for the band-to-band optical absorption edge of β-rhombohedral boron.

It is known that a surface amorphous layer usually leads to band tails or generates localized states in the bandgap of the semiconductor, depending on the thickness of the surface amorphous layer. For example, by engineering a 1 nm thick disordered surface layer on anatase TiO_2 nanocrystals,[6] the light-absorption onset of TiO_2 can be extended from around 400 nm in its pristine form to 1200 nm through the generation of band tails in the valence and conduction bands. In the case of the sub-micrometer-sized boron crystals with an around 2 nm thick surface amorphous layer, its absorption edge is actually not as steep as that of highly crystalline semiconductors[37] because of the band tails or midgap states caused by the surface amorphous layer. This claim is strongly supported by the obviously changed absorption edge when the surface amorphous layer is partially removed by etching with H_2 at 600 °C (see Figure S2). The edge is apparently blue-shifted after etching (Figure 5). Furthermore, the absorption

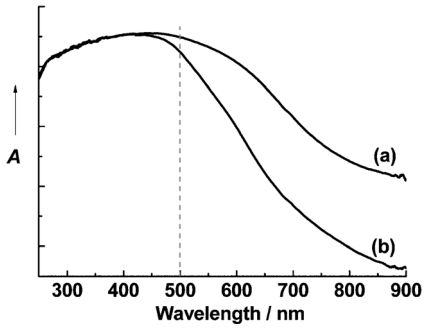

Figure 5. UV/Vis absorption spectra of the sub-micrometer-sized boron crystals a) before and b) after heating in an H_2 atmosphere at 600 °C for 3 h.

region between 500 and 800 nm becomes a shoulderlike band, whose origin could be the band tails or midgap states. We therefore propose that the absorption turning point that appears before 500 nm is related to the intrinsic band-to-band absorption edge of crystalline boron. Thus, the real bandgap of β-rhombohedral boron is probably larger than the previously reported 1.5–1.6 eV[32]. Further studies on determining the exact bandgap remains necessary.

The photocatalytic activity of elemental boron was estimated by monitoring its ability to generate ·OH radicals, an important active species in photocatalysis degradation,[38] under irradiation. It is known that terephthalic acid (TA) can react with an ·OH radical to generate 2-hydroxyterephthalic acid (TAOH), which gives a unique fluorescence emission peak centered at around 426 nm.[39] The clear emission signal associated with TAOH, generated in the suspension of sub-micrometer-sized boron in TA, increases monotonically with the irradiation time with visible light (Figure 6a). The nearly linear increase in the signal intensity at 426 nm indicates the good stability of the sub-micrometer-sized elemental boron as a photocatalyst (Figure 6b). These results suggest that elemental boron is indeed photocatalytically active in generating ·OH radicals under irradiation with visible light.

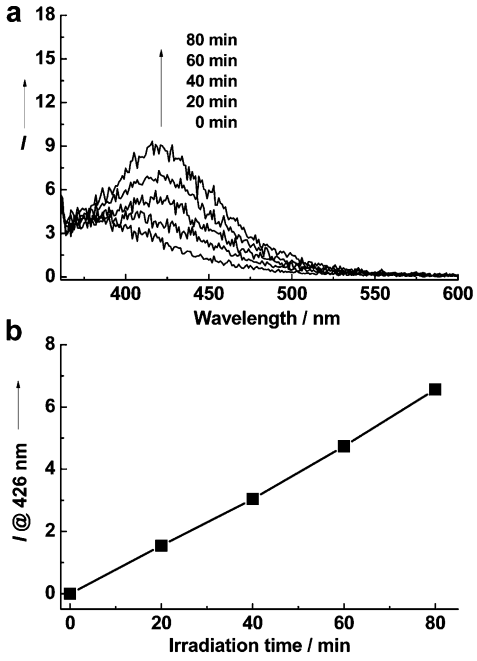

Figure 6. Estimation of photocatalytic activity: a) Time-dependent fluorescence emission spectra of TAOH generated in a suspension of the sub-micrometer-sized boron in TA under irradiation with visible light ($\lambda > 420$ nm). b) Time-dependent fluorescence-emission intensity of TAOH at 426 nm (the intensity values were normalized by setting the intensity value at 0 min as zero).

As demonstrated above, the direct bandgap at the Γ point exists in the β-rhombohedral elemental boron. Under visible light (> 420 nm), the bandgap at the Γ point can be excited. Therefore, the generation of TAOH under visible light is caused by band-to-band excitation at the Γ point; this process generates the photoexcited charge carriers to induce photocatalytic reactions.

We attempted to elucidate the role of the surface amorphous layer of the boron-rich oxide in the photocatalytic activity of β-rhombohedral elemental boron. The activity measurements suggest that the rate of TAOH generation with the sub-micrometer-sized boron under visible light is improved by a factor of 2.2 when the surface amorphous layer is partially removed by etching with H_2 (see Figure S3).

Furthermore, the rate of TAOH generation with the highly crystalline micrometer-sized boron is 1.3 times higher than that observed with the sub-micrometer-sized boron with a 2 nm thick surface amorphous layer (see Figure S4) despite the much larger particle size of the former than the latter (see Figure S5). These comparisons clearly indicate that the surface amorphous layer impairs the photocatalytic activity of elemental boron to a remarkable extent. This effect is observed because the surface amorphous layer, which usually generates band tails or localized midgap states, can lower both the mobility and redox potential of photoexcited charge carriers and thus increase charge-carrier recombination. It is therefore expected that the development of nanometer-sized elemental boron crystals without a surface amorphous layer (or at least the minimization of its thickness) could lead to high photoactivity. Currently, we are trying to optimize the etching process with H_2 with the purpose of minimizing the thickness of the amorphous layer. Further efforts will explore some strategies that have been used effectively to stabilize silicon-based photocatalysts and photoelectrodes.

Finally, we studied the chemical states of the boron photocatalysts before and after the photocatalytic reaction to estimate the stability of the photocatalysts. The B 1s XPS spectrum of the micrometer-sized boron photocatalyst was almost unchanged after the reaction (see Figure S6), which suggests the good stability of the boron photocatalysts.

Received: March 16, 2013
Published online: April 29, 2013

Keywords: boron · electronic structure · photocatalysis · semiconductors · visible light

[1] A. Fujishima, K. Honda, *Nature* **1972**, *238*, 37.
[2] M. Grätzel, *Nature* **2001**, *414*, 338.
[3] A. Kudo, Y. Miseki, *Chem. Soc. Rev.* **2009**, *38*, 253.
[4] R. Asahi, T. Morikawa, T. Ohwaki, K. Aoki, Y. Taga, *Science* **2001**, *293*, 269.
[5] a) H. G. Yang, C. H. Sun, S. Z. Qiao, J. Zou, G. Liu, S. C. Smith, H. M. Cheng, G. Q. Lu, *Nature* **2008**, *453*, 638; b) A. Selloni, *Nat. Mater.* **2008**, *7*, 613.
[6] X. B. Chen, L. Liu, P. Y. Yu, S. S. Mao, *Science* **2011**, *331*, 746.
[7] M. Batzill, *Energy Environ. Sci.* **2011**, *4*, 3275.
[8] Z. G. Zou, J. H. Ye, K. Sayama, H. Arakawa, *Nature* **2001**, *414*, 625.
[9] K. Maeda, K. Teramura, D. L. Lu, T. Takata, N. Saito, Y. Inoue, K. Domen, *Nature* **2006**, *440*, 295.
[10] P. Ritterskamp, A. Kuklya, M. A. Wustkamp, K. Kerpen, C. Weidenthaler, M. Demuth, *Angew. Chem.* **2007**, *119*, 7917; *Angew. Chem. Int. Ed.* **2007**, *46*, 7770.
[11] X. C. Wang, K. Maeda, A. Thomas, K. Takanabe, G. Xin, J. M. Carlsson, K. Domen, M. Antonietti, *Nat. Mater.* **2009**, *8*, 76.
[12] J. G. Tao, T. Luttrell, M. Batzill, *Nat. Chem.* **2011**, *3*, 296.
[13] X. X. Xu, C. Randorn, P. Efstathiou, J. T. S. Irvine, *Nat. Mater.* **2012**, *11*, 595.
[14] S. J. Wang, S. F. Swingle, H. Ye, F. R. F. Fan, A. H. Cowley, A. J. Bard, *J. Am. Chem. Soc.* **2012**, *134*, 11056.
[15] Z. Y. Zhang, Q. P. Lin, D. Kurunthu, T. Wu, F. Zuo, S. T. Zheng, C. J. Bardeen, X. H. Bu, P. Y. Feng, *J. Am. Chem. Soc.* **2011**, *133*, 6934.
[16] J. Liu, S. Wen, Y. Hou, F. Zuo, G. J. O. Beran, P. Feng, *Angew. Chem.* **2013**, *125*, 3323; *Angew. Chem. Int. Ed.* **2013**, *52*, 3241.
[17] X. B. Chen, S. H. Shen, L. J. Guo, S. S. Mao, *Chem. Rev.* **2010**, *110*, 6503.
[18] H. Tong, S. X. Ouyang, Y. P. Bi, N. Umezawa, M. Oshikiri, J. H. Ye, *Adv. Mater.* **2012**, *24*, 229.
[19] Z. H. Kang, C. H. A. Tsang, Z. D. Zhang, M. L. Zhang, N. Wong, J. Antonio Zapien, Y. Shan, S. T. Lee, *J. Am. Chem. Soc.* **2007**, *129*, 5326.
[20] F. Wang, W. K. H. Ng, J. C. Yu, H. J. Zhu, C. H. Li, L. Zhang, Z. F. Liu, Q. Li, *Appl. Catal. B* **2012**, *111–112*, 409.
[21] F. Wang, C. H. Li, Y. C. Li, J. C. Yu, *Appl. Catal. B* **2012**, *119–120*, 267.
[22] Y. D. Chiou, Y. J. Hsu, *Appl. Catal. B* **2011**, *105*, 211.
[23] G. Liu, P. Niu, L. C. Yin, H. M. Cheng, *J. Am. Chem. Soc.* **2012**, *134*, 9070.
[24] G. Liu, P. Niu, H.-M. Cheng, *ChemPhysChem* **2013**, *14*, 885.
[25] *Popular Library of the Elements* (Ed.: I. V. Petryanov-Sokolov), Nauka, **1983**, chap. 5.
[26] M. I. Eremets, V. V. Struzhkin, H. K. Mao, R. J. Hemley, *Science* **2001**, *293*, 272.
[27] A. R. Oganov, J. H. Chen, C. Gatti, Y. Z. Ma, Y. M. Ma, C. W. Glass, Z. X. Liu, T. Yu, O. O. Kurakevych, V. L. Solozhenko, *Nature* **2009**, *457*, 863.
[28] N. N. Greenwood, A. Earnshaw, *Chemistry of the Elements*, Reed Educational and Professional Publishing Ltd, UK, **1997**, p. 139.
[29] M. J. van Setten, M. A. Uijttewaal, G. A. de Wijs, R. A. de Groot, *J. Am. Chem. Soc.* **2007**, *129*, 2458.
[30] M. Widom, M. Mihalkovic, *Phys. Rev. B* **2008**, *77*, 064113.
[31] T. Ogitsu, F. Gygi, J. Reed, Y. Motome, E. Schwegler, G. Galli, *J. Am. Chem. Soc.* **2009**, *131*, 1903.
[32] H. Werheit, M. Laux, U. Kuhlmann, *Phys. Status Solidi B* **1993**, *176*, 415.
[33] T. T. Xu, J. G. Zheng, N. Q. Wu, A. W. Nicholls, J. R. Roth, D. A. Dikin, R. S. Ruoff, *Nano Lett.* **2004**, *4*, 963.
[34] R. E. Hughes, C. H. L. Kennard, D. B. Sullenger, H. A. Weakliem, D. E. Sands, J. L. Hoard, *J. Am. Chem. Soc.* **1963**, *85*, 361.
[35] G. A. Slack, C. I. Hejna, J. S. Kasper, *J. Solid State Chem.* **1988**, *76*, 52.
[36] M. Widom, M. Mihalkovič, *Phys. Rev. B* **2008**, *77*, 064113.
[37] G. Liu, L. Z. Wang, C. H. Sun, X. X. Yan, X. W. Wang, Z. G. Chen, S. C. Smith, H. M. Cheng, G. Q. Lu, *Chem. Mater.* **2009**, *21*, 1266.
[38] M. R. Hoffmann, S. T. Martin, W. Choi, D. W. Bahnemann, *Chem. Rev.* **1995**, *95*, 69.
[39] T. Hirakawa, Y. Nosaka, *Langmuir* **2002**, *18*, 3247.

